Oxide Film Characterization of Fe-based Alloys for Potential Accident Tolerant Fuel Application in Simulated PWR Environment

Su Hyun Park[a], Chaewon Kim[a], Chae Won Jeong[a], Hyeon Bae Lee[a], Changheui Jang[a,*]
[a]Korea Advanced Institute of Science and Technology, Daejeon, Korea
[*]Corresponding author: chjang@kaist.ac.kr

1. Introduction

Since the Fukushima accident in March 2011, there were many efforts to establish the integrity of fuel claddings with enhanced accident tolerance. Many studies focused on reducing the hydrogen generation rate and the heat generated by oxidation of zirconium alloy (Zircaloy) cladding. Meanwhile, the Fe-base alloys have been proposed as a potential accident tolerant fuel (ATF) cladding to replace zirconium alloys because of the corrosion resistance [1-4]. Under this circumstance, authors' group has developed model alumina-forming duplex stainless steel (ADSS) alloys to remedy the weakness, and details were reported in the other references [5,6].

The performance of the developed alloy #B51 should be maintained during normal operations and operational transients as well as the loss of coolant accident in the reactor core. In this study, the corrosion behaviors of #B51 ADSS were evaluated by oxide film observation. The oxide film formed in simulated typical pressurized water reactor (PWR) primary water environment has been investigated by observation of oxide morphology and electrochemically characterization.

2. Experimental

2.1 Test material

The #B51 ADSS and commercial alloys including 347 stainless steel (SS), APM, and 2205 (DSS) are used in this study. The 347 SS (which has similar chromium content with #B51), APM (alumina forming alloy), and 2205 (duplex stainless steel) are chosen as the reference materials. The chemical compositions of used material were analyzed by using the inductively coupled plasma atomic emission spectroscopy (ICP-AES), and the results are summarized in Table 1. The materials were machined as coupon specimens, which have diameter of 15 mm with a hole (1 mm diameter) and thickness of 1 mm, then surfaces were mechanically polished by using 1 μm diamond paste.

2.2 Immersion test condition

The immersion test of coupon specimens was performed in simulated PWR primary water environment that test system consists of the re-circulated loop as shown in Fig. 1. The temperature and pressure are maintained during the immersion test at 400 ℃ and 20 MPa, respectively. To achieve the target temperature and control within ± 1 ℃, the pre heater and main heater were installed in front of autoclave and directly attached to autoclave, respectively. The test solution is prepared by mixing the distilled water with 1200 ppm of boric acid (H_3BO_3) and 2.2 ppm of lithium hydroxide (LiOH), which has the conductivity of 22 – 25 μS/cm. The prepared solution is stored in 1st and 2nd column as shown in Fig. 1. The two type of gas were used to achieve the target dissolved oxygen (DO) and dissolved hydrogen (DH) concentration. The argon gas is purged at 1st column to decrease the DO concentration below the 5 ppb and the hydrogen has is purged at 2nd column to decrease DO together and reach to 25 cc/kg-H_2O of DH concentration as well. It should be note that the 2nd column is pressurized at approximately 0.9 bar to achieve the target DH concentration. The test condition is summarized in Table 2, and all parameters of inlet and outlet solution were monitored and kept during the test.

Fig. 1. The schematic of test loop system used in this study.

Table I: Chemical compositions of test materials used in this study.

Compositions [wt.%]	Fe	Cr	Ni	C	Mn	Si	Nb	Al
ADSS #B51	Bal.	16.33	18.77	0.11	1.04	0.31	0.53	6.14
347 S	Bal.	17.25	10.22	0.03	1.68	0.4	0.28	
APM	Bal.	21.99	0.15	0.03	0.16	0.28		5.81
2205	Bal.	22.5	4.8	0.01	0.87	0.45		

Table II: Water chemistry of simulated PWR environment.

Environment		Simulated PWR steam
Temperature		400 ºC
Pressure		20 MPa
Water chemistry	Dissolved hydrogen	25 cc/kg
	Dissolved oxygen	< 5 ppb
	Conductivity	22-26 µS/cm

2.3 Oxide film observation and measurement

The coupon specimens were exposed to simulated PWR environment up to 1300 hours, and their weight changes were measured at the immersion time of 0, 400, 800, and 1300 hours, respectively.

The oxide morphology was observed by using field emission scanning electron microscopy (FE-SEM) equipped with energy dispersive spectroscopy (EDS). Further analyses for cross sectional observation were performed by using focused ion beam (FIB) and transmission electron microscopy (TEM). The chemical distribution of oxide film of test materials is measured in scanning transmission electron microscopy (STEM) mode.

To measure the semiconductor properties of oxide films, the electrochemical method is used in this study. The coupon specimens were electrically connected with metal wire, then all surfaces were covered with silicon for sealant except for one side of surface only for measuring electrochemical properties. The measurements were performed by using typical three-electrode system, which consists of a saturated calomel electrode (SCE) as a reference electrode and a small platinum plate as a counter electrode. The electrochemical impedance spectroscopy (EIS) is measured at open circuit potential (OCP) state in borated buffer solution (0.05 M H_3BO_3 + 0.075 M $Na_2B_4O_7$) with 9.2 pH. The AC amplitude of 10 mV and the frequency from 1kHz to 0.1 Hz were used to obtain the EIS. Moreover, the Mott-Shottky (M-S) analysis, which is a useful method to measure the defect density of oxide film, was subsequently conducted by potential scanning from -0.6 V (SCE) to + 0.6 V (SCE) with scan rate of 10 mV. The capacitance was measured in a frequency of 1 kHz with ac amplitude of 10 mV.

3. Results

3.1 Weight changes and oxide morphology observation

The weight changes were measured at the immersion time of 0, 400, 800, and 1300 hours, and the results are shown in Fig. 2. It should be note that the weight change data of 1300 hour of immersion is not included yet. All specimens show weight gain after 800 hours of immersion. Especially, the amount of weight gain of

#B51 ADSS and 347 SS is relatively higher than that of 2205 DSS and APM alloys.

Figure 3 shows the surface oxide morphologies of test materials formed in simulated PWR environment for 400 hours. Oxide morphologies of #B51 ADSS and 347 SS are covered with well-developed oxide particles compared with the surface of 2205 DSS and APM alloys, which could support the weight change results of Fig. 2. The point analyses for chemical composition measurement were performed on the surface oxide, and results are briefly shown with white arrows. The point analyses of #B51 ADSS and 347 SS indicate that the surface is covered with Fe-rich oxide, otherwise, the results of 2205 DSS and APM show Fe and Cr-rich oxide and Fe-rich oxide depends on location. The big particles on surface are mostly composed of Fe-rich oxide and Cr-rich oxide appears in locations where the oxide film looks thin. Moreover, the surface of 2205 DSS could be separated by 2 section whether the surface is covered by oxide or not. This is thought due to the phase distribution of ferrite and austenite. Ferrite has higher Cr content because Cr has bcc crystal structure and it is well known as a ferrite stabilizer. Thus, ferrite has higher corrosion resistance and the corrosion rate is slower than the austenite phase [7]. Meanwhile, the #B51 ADSS has also duplex phase, so it could be separate into two area depends on surface coverage of oxide particles. However, it is not clear as 2205 DSS, and thought that due to the lower Cr content than 2205 DSS. In addition, the APM also shows similar tendency with 2205 DSS, which is composed of ferrite single phase. This uneven surface morphology could be thought that the time dependent property, which means that the corrosion rate is slow because of the high Cr content in ferrite phase, and the number of oxide particles observed on the surface appears small and uneven.

The TEM observation of oxide film of test materials formed in simulated PWR environment will be performed.
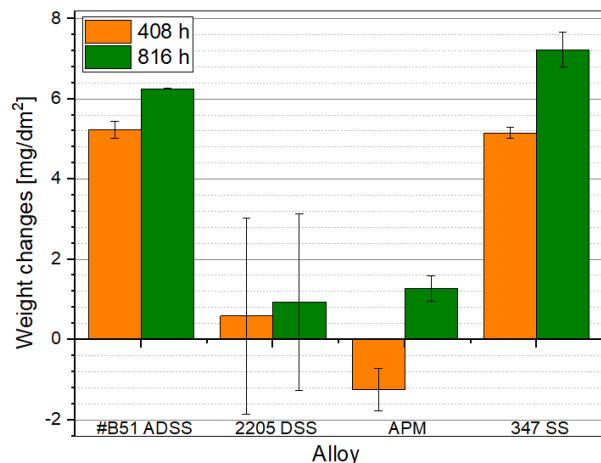
Fig. 2. The weight changes of test materials at the immersion time of 0, 400, and 800 hours.
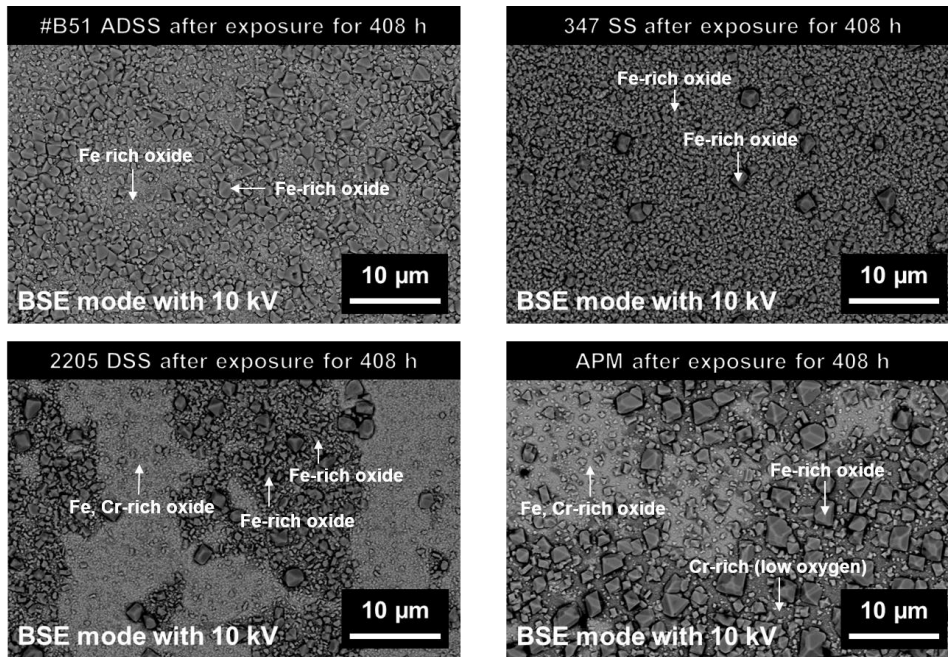
Fig. 3. The results of surface oxide observation of test materials exposed to simulated PWR environment for 400 hours.

3.2 Electrochemical properties measurement

The measurement of electrochemical properties of oxide films of test materials formed in simulated PWR environment is under on-going. The data will be prepared and presented.

4. Conclusion

The corrosion behaviors of developed material #B51 ADSS are evaluated compared with commercial alloys such as 347 SS, 2205 DSS, and APM alloys.

- The weight changes of test materials mostly depend on Cr content in materials. Similar weight gain was observed for #B51 ADSS and 347 SS.
- The surface oxide morphology changes depending on Cr content also. Even though, the #B51 ADSS and 2205 DSS have both ferrite and austenite structure, less corroded surface is observed in ferrite phase of 2205 DSS because of higher Cr content.
- The results of oxide observation by using TEM would be prepared.
- The results of electrochemical analyses of EIS and MS would be prepared.

REFERENCES

[1] D. J. Park, H. G. Kim, Y. I. Jung, J. H. Park, and Y. H. Koo, Behavior of an improved Zr fuel cladding with oxidation resistant coating under loss-of-coolant accident conditions, Journal of Nuclear Materials, 482(2016), pp. 75-82.
[2] B. A. Pint, K. A. Terrani, Y. Yamamoto, and L. L. Snead, Material selection for accident for accident tolerant fuel cladding, Metallurgical and Materials and Transactions E, 2(2015), pp. 190-196.
[3] Y. Yamamoto, B. A. Pint, K. A. Terrani, K. G. Field, Y. Yang, and L. L. Snead, Development and property evaluation of nuclear grade wrought FeCrAl fuel cladding for light water reactors, Journal of Nuclear Materials, 467(2015), pp. 703-716.
[4] K. A. Terrani, S. J. Zinkle, L. L. Snead, Advanced oxidation-resistant iron-based alloys for LWR fuel cladding, Journal of Nuclear Materials, 448(2014), pp. 420-435.
[5] H. Kim, H. Jang, G. O. Subramanian, C. Kim, and C. Jang, Development of alumina-forming duplex stainless steels as accident-tolerant fuel cladding materials for light water reactors, Journal of Nuclear Materials, 507(2018), pp. 1-14.
[6] C. Kim, H. Kim, C. Jang, K. Kim, Y. Kim, S. Lee, and H. Jang, Feasibility assessment of the alumina-forming duplex stainless steels as accident tolerant fuel cladding materials for light water reactors, International Journal of Energy Research, 2020;44:8074-8088.
[7] M. Langberg et al., Characterization of Native Oxide and Passive Film on Austenite/Ferrite Phases of Duplex Stainless Steel Using Synchrotron HAXPEEM, Journal of The Electrochemical Society, 166, 2019.